

1 **Graphene oxide based ultrafiltration membranes for photocatalytic degradation**  
2 **of organic pollutants in salty water**

3

4 Luisa M. Pastrana-Martínez, Sergio Morales-Torres, José L. Figueiredo, Joaquim L. Faria,  
5 Adrián M.T. Silva\*

6 *LCM – Laboratory of Catalysis and Materials – Associate Laboratory LSRE/LCM, Faculdade*  
7 *de Engenharia, Universidade do Porto, Rua Dr. Roberto Frias, 4200-465 Porto, Portugal.*

8

9

10 \*Corresponding author: [adrian@fe.up.pt](mailto:adrian@fe.up.pt); Tel: +351-22-0414908

11

12

13

14

15

16

17

18

19

20

21

22

23

24

25

26 **Abstract**

27 Flat sheet ultrafiltration (UF) membranes with photocatalytic properties were prepared with  
28 lab-made TiO<sub>2</sub> and graphene oxide-TiO<sub>2</sub> (GOT), and also with a reference TiO<sub>2</sub> photocatalyst  
29 from Evonik (P25). These membranes were tested in continuous operation mode for the  
30 degradation and mineralization of a pharmaceutical compound, diphenhydramine (DP), and  
31 an organic dye, methyl orange (MO), under both near-UV/Vis and visible light irradiation.  
32 The effect of NaCl was investigated considering simulated brackish water (NaCl 0.5 g L<sup>-1</sup>)  
33 and simulated seawater (NaCl 35 g L<sup>-1</sup>). The results indicated that the membranes prepared  
34 with the GOT composite (M-GOT) exhibited the highest photocatalytic activity,  
35 outperforming those prepared with bare TiO<sub>2</sub> (M-TiO<sub>2</sub>) and P25 (M-P25), both inactive under  
36 visible light illumination. The best performance of M-GOT may be due to the lower band-gap  
37 energy (2.9 eV) of GOT. In general, the permeate flux was also higher for M-GOT probably  
38 due to a combined effect of its highest photocatalytic activity, highest hydrophilicity (contact  
39 angles of 11°, 17° and 18° for M-GOT, M-TiO<sub>2</sub> and M-P25, respectively) and higher porosity  
40 (71%). The presence of NaCl had a detrimental effect on the efficiency of the membranes,  
41 since chloride anions can act as hole and hydroxyl radical scavengers, but it did not affect the  
42 catalytic stability of these membranes. A hierarchically ordered membrane was also prepared  
43 by intercalating a freestanding GO membrane in the structure of the M-GOT membrane (M-  
44 GO/GOT). The results showed considerably higher pollutant removal in darkness and good  
45 photocatalytic activity under near-UV/Vis and visible light irradiation in continuous mode  
46 experiments.

47

48 **Keywords:** *Graphene oxide; photocatalytic membranes; filtration; water purification; salty*  
49 *water; anti-fouling.*

50

## 51 **1. Introduction**

52 The scarcity of clean water and increasing environmental pollution are critical issues in large  
53 and industrialized cities as well as in less developed regions. In this context, efficient water  
54 purification technologies with low energy consumptions are needed (Shannon et al. 2008).  
55 Membranes play a key role in water purification, seawater and brackish water desalination as  
56 well as in wastewater reclamation and reuse (Pendergast and Hoek 2011, Peters 2010). The  
57 preparation of appropriate membranes is an important step, and different materials, such as  
58 polymers, ceramics and carbon nanotubes, have been successfully employed (Baek et al.  
59 2014, Das et al. 2014, Ulbricht 2006, Xu et al. 2013b). Fouling is one of the major problems  
60 affecting the performance of these membranes.

61 In recent years, membranes prepared with photocatalytic nanoparticles have attracted great  
62 attention due to their superior characteristics (e.g., anti-fouling and photocatalytic properties)  
63 when compared to conventional membranes (Kim and Van der Bruggen 2010). Titanium  
64 dioxide (TiO<sub>2</sub>) is one of the most widely used photocatalysts due to its low cost, chemical and  
65 thermal stability and excellent photoactivity (Chen and Mao 2007). Up to date, various TiO<sub>2</sub>-  
66 based photocatalytic membranes have been studied (Albu et al. 2007, Pan et al. 2008, Zhang  
67 et al. 2006, Zhang et al. 2014b). However, the suppression of the recombination of photo-  
68 generated charge carriers, as well as the effective utilization of visible light, are some of the  
69 main challenges before these membranes become economically feasible.

70 Graphene and its derivatives, such as graphene oxide (GO), have attracted huge attention in  
71 photocatalytic applications (Tu et al. 2013). GO is a material that can be easily produced by  
72 chemical oxidation and exfoliation of graphite. In addition, it can be easily manipulated and  
73 its oxygen-containing functional groups (hydroxyl and epoxy groups on the basal planes, and  
74 carboxyl and carbonyl groups on the edges) facilitate the interaction of GO sheets with a wide  
75 variety of organic and inorganic materials (Dreyer et al. 2010, Pastrana-Martínez et al. 2014).

76 GO-TiO<sub>2</sub> composites are efficient photocatalysts under both near-UV/Vis and visible light  
77 irradiation, overcoming one of the main limitations of bare TiO<sub>2</sub> (Amalraj Appavoo et al.  
78 2014, Fan et al. 2011, Huang et al. 2014, Long et al. 2013, Pastrana-Martínez et al. 2013a,  
79 Pastrana-Martínez et al. 2014, Pastrana-Martínez et al. 2012). However, these materials are  
80 usually employed as suspended particles (slurries) in batch reactors and, thus, a second step is  
81 required for catalyst separation from the treated water, limiting its recovery and reuse.

82 The immobilization of the photocatalyst into/onto filtration membranes/fibres overcomes this  
83 problem, but only a few works have been published on this topic (Athanasakou et al. 2014,  
84 Gao et al. 2013, Gao et al. 2014, Pastrana-Martínez et al. 2013b). A GO-TiO<sub>2</sub> microsphere  
85 hierarchical membrane was developed by assembling the photocatalyst on the surface of a  
86 cellulose acetate filtration membrane, which showed the multifunctionality of water filtration  
87 and photodegradation of acid orange 7 and rhodamine B (Gao et al. 2013). A GO-TiO<sub>2</sub>  
88 photocatalytic membrane was synthesized by simple layer-by-layer deposition of TiO<sub>2</sub> and  
89 GO on a polysulfone membrane, and the increase in the membrane flux was attributed to the  
90 photo-enhanced hydrophilicity and simultaneous degradation of the methylene blue model  
91 pollutant (Gao et al. 2014). Recently, we immobilized a highly active GO-TiO<sub>2</sub> composite  
92 into alginate hollow fibres by a dry/wet spinning process, and considerable high  
93 photocatalytic activity and stability for degradation of diphenhydramine were observed in  
94 consecutive light–dark cycles of continuous operation (Pastrana-Martínez et al. 2013b). This  
95 composite was also immobilized onto ceramic monoliths via dip-coating and tested as a  
96 hybrid photocatalysis/ultrafiltration process for the removal of methyl orange and methylene  
97 blue dyes, the membranes exhibiting enhanced photocatalytic performance under visible light  
98 (Athanasakou et al. 2014). GO-TiO<sub>2</sub> composite membranes were also prepared for exclusive  
99 use as filtration membranes (i.e. without photocatalysis involved ) to remove hazardous dyes,  
100 such as methyl orange and rhodamine B (Xu et al. 2013a).

101 In the present work, three photocatalysts, i.e. lab-made bare TiO<sub>2</sub> and GO-TiO<sub>2</sub>, as well as the  
102 reference material in photocatalysis, Evonik Degussa (P25), were assembled on flat sheet  
103 filtration cellulose membranes. The resulting photocatalytic ultrafiltration membranes were  
104 tested for the photodegradation and mineralization of a pharmaceutical compound,  
105 diphenhydramine (DP), and an organic dye, methyl orange (MO), under both near-UV/Vis  
106 and visible light irradiation and in continuous operation mode. In addition, an innovative  
107 freestanding GO membrane was intercalated between the cellulose membrane and the  
108 photocatalytic layer. Besides studies with the model pollutants in distilled water (DW), the  
109 effect of the presence of Cl<sup>-</sup> anions on the removal of the pollutants was also studied in  
110 simulated brackish water (SBW) and seawater (SSW).

111

## 112 **2. Experimental**

### 113 *2.1. Chemicals and materials*

114 Natural graphite (99.9995%), diphenhydramine hydrochloride (C<sub>17</sub>H<sub>21</sub>NO·H<sub>2</sub>O, 99%), methyl  
115 orange (C<sub>14</sub>H<sub>14</sub>N<sub>3</sub>NaO<sub>3</sub>S, 99%), ammonium hexafluorotitanate ((NH<sub>4</sub>)<sub>2</sub>TiF<sub>6</sub>, 99.99%) and  
116 boric acid (H<sub>3</sub>BO<sub>3</sub>, 99%), were obtained from Sigma-Aldrich. Sodium chloride (NaCl, 99.5%)  
117 was supplied by Panreac. Mixed cellulose ester (MCE) membranes with 0.45 μm pore size,  
118 diameter of 4.7 cm and thickness of 140 μm were purchased from Whatman<sup>TM</sup>. The  
119 commercial TiO<sub>2</sub> material (P25) was supplied by Evonik Degussa Corporation (P25) and was  
120 used as reference material. It is constituted by 80% of anatase phase and 20% of rutile  
121 (manufacturer data).

122

### 123 *2.2. Synthesis of graphene oxide and GO-TiO<sub>2</sub>*

124 Graphite oxide was obtained by the oxidative treatment of commercial graphite (20 μm,  
125 Sigma-Aldrich) following the modified Hummers method, as described elsewhere (Hummers

126 and Offeman 1958, Pastrana-Martínez et al. 2012). The oxidized material was dispersed in  
127 water, sonicated for 1 h and centrifugated at 3000 r.p.m. to obtain a suspension of graphene  
128 oxide (GO).

129 GO-TiO<sub>2</sub> (hereafter referred as GOT) was prepared by liquid phase deposition method  
130 according to our previous work (Pastrana-Martínez et al. 2012). Briefly, (NH<sub>4</sub>)<sub>2</sub>TiF<sub>6</sub> (0.1 mol  
131 L<sup>-1</sup>) and H<sub>3</sub>BO<sub>3</sub> (0.3 mol L<sup>-1</sup>) were added to a GO dispersion that was then heated at 60 °C for  
132 2 h under vigorous stirring. Then the resulting powder was treated at 200 °C under N<sub>2</sub> flow.  
133 The carbon loading (~ 4.0 wt.%) was selected taking into account the composite presenting  
134 the highest photocatalytic activity under UV/Vis and visible light irradiation in our previous  
135 work (Pastrana-Martínez et al. 2012). Bare TiO<sub>2</sub> was prepared using the same methodology  
136 but without the addition of GO (hereafter referred as TiO<sub>2</sub>).~~The photocatalyst from Evonik~~  
137 ~~Degussa Corporation (P25) was also used as reference material~~ The synthesis of GO, TiO<sub>2</sub>  
138 and GO-TiO<sub>2</sub> composite are shown in Scheme 1.

139

### 140 2.3. Preparation of photocatalytic membranes

141 GOT, TiO<sub>2</sub> and P25 catalysts were selected to prepare the corresponding photocatalytic  
142 membranes following a methodology adapted from elsewhere (Morales-Torres et al. 2014), in  
143 that case for the preparation of CNT buckypapers over a polytetrafluoroethylene commercial  
144 membrane. In a typical procedure, the photocatalyst was dispersed in a 2 g L<sup>-1</sup> aqueous  
145 solution during 10 min by using an ultrasonic processor (UP400S, 24 kHz). The MCE  
146 membrane was cut into a piece with 1.4 cm of diameter and placed into a filtration device  
147 under vacuum. 5 mL of the photocatalyst dispersion was added slowly (ca. 10 mg of  
148 photocatalyst). When the filtration was completed, the membrane was dried under N<sub>2</sub> flow for  
149 10 min, a homogeneous deposition of the photocatalyst being obtained with an effective area

150 of ca. 1.54 cm<sup>2</sup>. The membranes prepared with GOT, TiO<sub>2</sub> and P25 were labelled as M-GOT,  
151 M-TiO<sub>2</sub> and M-P25, respectively.

152 The membrane presenting the highest photocatalytic activity was also modified by  
153 intercalating a freestanding GO membrane between the MCE membrane and the photocatalyst  
154 layer. First, 2 mL of GO dispersion (1.5 g L<sup>-1</sup>) was filtered through a MCE membrane, and a  
155 homogeneous GO layer was obtained above the MCE membrane (labelled as M-GO). Then, a  
156 uniform multi-layer membrane was prepared by adding 5 mL of the GOT composite  
157 suspension (2 g L<sup>-1</sup>) on top of the M-GO membrane (M-GO/GOT).

158

#### 159 2.4. Characterization techniques

160 The morphology and roughness of the membranes were analysed by scanning electron  
161 microscopy (SEM) using a FEI Quanta 400FEG ESEM/EDAX Genesis X4M instrument. The  
162 membranes were frozen and broken under liquid nitrogen. The microscope was equipped with  
163 a special multiple sample holder, in which the broken membranes were vertically positioned  
164 to analyze their cross-sections.

165 The overall porosity ( $\varepsilon$ ) of the membranes was determined by the gravimetric method (Cui et  
166 al. 2013). After measuring the dry weight of the membranes, they were immersed in distilled  
167 water overnight to assure solvent penetration into the membrane pores. Then, their wet weight  
168 was registered. The porosity was calculated by applying the following equation:

$$169 \quad \varepsilon (\%) = \frac{(m_w - m_d) / \rho_w}{(m_w - m_d) / \rho_w + m_d / \rho_p} \times 100 \quad (1)$$

170 where  $m_w$  and  $m_d$  are the weights of the wet and dry membranes, respectively, and  $\rho_w$  and  $\rho_p$   
171 are the water (0.997 g cm<sup>-3</sup>) and polymer (1.520 g cm<sup>-3</sup>) densities, respectively (Maim et al.  
172 1947). Four different membranes were used to determine an average value of the porosity,  
173 and the standard deviation found was always lower than  $\pm 1\%$ .

174 N<sub>2</sub> adsorption-desorption isotherms at -196 °C were obtained in a Quantachrome NOVA  
175 4200e multi-station apparatus. The apparent surface area ( $S_{\text{BET}}$ ) was determined by applying  
176 the Brunauer–Emmett-Teller (BET) equation (Brunauer et al. 1938). The volume of N<sub>2</sub>  
177 adsorbed at a relative pressure of 0.95 ( $V_p$ ) was obtained from the adsorption isotherms,  
178 which corresponds to the sum of the micro- and mesopore volumes according to Gurvitch’s  
179 rule (Rouquerol et al. 1999). The the Barrett-Joyner-Halenda (BJH) method (Barrett et al.  
180 1951) was applied to the desorption branch of the N<sub>2</sub> isotherms to determine the average  
181 mesopore diameter ( $d_{\text{pore}}$ ).

182 The hydrophilicity of the membrane surface was determined by contact angle ( $\theta$ )  
183 measurements using an Attension apparatus (model Theta) that allowed image acquisition and  
184 data analysis. The measurements were performed at room temperature (25 °C) using the water  
185 drop method on dry membranes. The contact angle was measured at least in 5 different  
186 locations to get the average value.

187 The optical properties of the samples were analyzed by UV/Vis diffuse reflectance  
188 spectroscopy using a JASCO V-560 UV/Vis spectrophotometer, equipped with an integrating  
189 sphere attachment (JASCO ISV-469), barium sulphate being used as reference. The  
190 reflectance spectra were converted to equivalent absorption Kubelka-Munk units by the  
191 instrument software (JASCO). The band-gap was determined by plotting the transformed  
192 Kubelka-Munk values as a function of the energy of light.

193 The materials point of zero charge ( $\text{pH}_{\text{PZC}}$ ) was determined following a pH drift test described  
194 elsewhere (Pastrana-Martínez et al. 2013b). Briefly, solutions with varying initial pH (2-12)  
195 were prepared using HCl (0.1 mol L<sup>-1</sup>) or NaOH (0.1 mol L<sup>-1</sup>) and 50 mL of NaCl (0.01 mol  
196 L<sup>-1</sup>) as electrolyte. Each solution was contacted with 0.15 g of the material and the final pH  
197 was measured after 24 h of continuous stirring at room temperature. The  $\text{pH}_{\text{PZC}}$  of the material



198 was determined by intercepting the obtained final-pH vs. initial-pH curve with the straight  
199 line final-pH = initial-pH.

200

### 201 2.5. *Evaluation of membranes performance*

202 The photocatalytic activity and permeability of the membranes were studied in dead-end  
203 filtration mode at ambient temperature (25 °C) and pressure under near-UV/Vis and visible  
204 light irradiation, using a lab-scale set up represented in Figure 1. The system consists of a  
205 glass made cylindrical reactor with the membrane attached by using a Viton® o-ring  
206 (maintaining the effective area of ca. 1.54 cm<sup>2</sup>). A reservoir containing the fresh pollutant  
207 solution was magnetically stirred and continuously purged with air flow. DP (3.40×10<sup>-5</sup> mol  
208 L<sup>-1</sup>) and MO (3.05×10<sup>-5</sup> mol L<sup>-1</sup>) were used as model pollutants in distilled water (DW) at  
209 natural pH conditions (pH<sub>DP</sub> = 5.9 and pH<sub>MO</sub> = 6.1). Experiments were also performed using  
210 simulated brackish water (SBW, 0.5 g L<sup>-1</sup> of NaCl) and seawater (SSW, 35 g L<sup>-1</sup> of NaCl).  
211 The pollutant solution was continuously introduced in the reactor at a flow rate of ca. 0.25 mL  
212 min<sup>-1</sup> using a peristaltic pump. This flow rate allows an adequate residence time into the  
213 reactor and was selected from preliminary studies at different flow rates. In a typical run, the  
214 solution was passed through the reactor for a long time (up to 180 min) before turning on the  
215 lamp, to saturate the membrane with the tested pollutants (ca. 60 min needed) and to achieve  
216 the initial pollutant concentration in the reactor outlet (i.e.  $C_{180 \text{ min in dark}} = C_{0 \text{ min under radiation}}$ ). In  
217 the particular case of the M-GO/GOT membranes a total of 48 h dark period was needed  
218 before turning on the lamp.

219 The irradiation source consisted of a Heraeus TQ 150 medium-pressure mercury vapour lamp.  
220 A DURAN® glass water cooling jacket was used to obtain irradiation in the near-UV  
221 irradiation ( $\lambda > 350 \text{ nm}$ ) and to control the operating temperature. A cut-off long pass filter  
222 was used ( $\lambda > 430 \text{ nm}$ ) for visible light experiments. The photon flow entering the reactor was

223 ca. 33 mW cm<sup>-2</sup> and 2.8 mW cm<sup>-2</sup> under near-UV/Vis and visible light irradiation,  
224 respectively, as determined by integrating the irradiance spectra obtained by using a UV/Vis  
225 spectroradiometer (USB2000+, OceanOptics, USA). In the photocatalytic experiments, two  
226 dark/bright cycles were carried out in order to evaluate the anti-fouling properties of the  
227 membranes. 2 mL of sample were systematically collected from the exit of the photocatalytic  
228 membrane reactor (i.e. before the permeate reservoir) at intervals of ca. 20 min, in order to  
229 measure the pollutant concentration. Blank experiments were also performed in the absence of  
230 catalyst in order to characterize direct photolysis and the filtration capacity of the commercial  
231 MCE membrane.

232 The concentration of DP was determined by HPLC with a Hitachi Elite LaChrom system  
233 equipped with a Hydrosphere C18 column. The concentration of MO was determined by UV-  
234 Vis spectrophotometry at 464 nm in a Jasco V-560 spectrophotometer. The total organic  
235 carbon (TOC) was determined for selected samples using a Shimadzu TOC-5000A analyzer.  
236 Chloride ions were monitored by ion chromatography (Metrohm 881 Compact IC) using a  
237 Metrosep A Supp 7-250 column.

238 The permeate flux (L m<sup>-2</sup> h<sup>-1</sup>) was calculated according to the following equation:

239 
$$F = \frac{V}{A \times t} \quad (2)$$

240 where  $V$  (L) is the volume of the solution permeated during the experiment,  $A$  represents the  
241 effective membrane area (m<sup>2</sup>), and  $t$  denotes time (h).

242

### 243 **3. Results and discussion**

#### 244 *3.1. Membranes characterization*

245 The cross-section and top view of the prepared membranes were analysed by SEM. The  
246 corresponding images of M-TiO<sub>2</sub> and M-GOT at different magnifications are shown in

247 Figures 2a-c and 2d-f, respectively. The total thicknesses of the membranes are gathered in  
248 Table 1.

249 Cross-sectional images of M-TiO<sub>2</sub> and M-GOT membranes (Figures 2a-b and 2d-e,  
250 respectively) show that the corresponding photocatalytic materials (top) were homogeneously  
251 deposited on the MCE membrane (bottom) without appreciable presence of cracks, holes or  
252 another defects, even if considered that these membranes were fractured for SEM analysis.  
253 Both membranes (M-TiO<sub>2</sub> and M-GOT) showed some differences in the packing and  
254 morphology of the deposited material. M-TiO<sub>2</sub> (Figures 2a-b and Table 1) presented a good  
255 distribution of TiO<sub>2</sub> particles on the substrate membrane with a uniform thickness of TiO<sub>2</sub>  
256 around 35 μm, while the overall thickness of the M-TiO<sub>2</sub> membrane was ~ 175 μm (ca. 140  
257 μm for MCE only). The top view of the M-TiO<sub>2</sub> membrane (Figure 2c) shows spherical  
258 particles forming larger aggregates with anatase crystallites of around 4-5 nm in size  
259 (Pastrana-Martínez et al. 2012).

260 The cross-sectional images of the M-GOT membrane (Figures 2d-e) show a uniform GOT  
261 layer deposited on the MCE membrane with a thickness of ~ 65 μm, almost twice as that  
262 observed for TiO<sub>2</sub> in the case of M-TiO<sub>2</sub>. The amount of photocatalyst deposited in both  
263 membranes was the same. Therefore, the larger thickness observed for M-GOT can be  
264 attributed to the lower density of the GOT catalyst (resulting from the arrangement of the  
265 GOT platelets, as shown in Figure 2f inset), which differs from that of TiO<sub>2</sub> spherical  
266 particles. The top view of the GOT composite (Figure 2f) indicates a good TiO<sub>2</sub> distribution  
267 on both sides of the GO sheets, i.e. a good self-assembly of the TiO<sub>2</sub> nanoparticles on GO  
268 (Pastrana-Martínez et al. 2012).

269 Regarding the M-P25 membrane (images not shown), a homogeneous layer of P25 with a  
270 thickness of ~ 39 μm (more similar to M-TiO<sub>2</sub> than to M-GOT) was observed over the MCE  
271 membrane, with a typical morphology of joined P25 nanoparticles.

272 The total porosity ( $\epsilon$ ) of the membranes was determined by the gravimetric method and the  
273 results are collected in Table 1. The porosity of the modified membranes (65-71%) was lower  
274 than that determined for the MCE membrane (74%), but that of M-GOT was the nearest to  
275 MCE (71%). The BET surface area ( $S_{\text{BET}}$ ) values were comparable for M-GOT ( $117 \text{ m}^2 \text{ g}^{-1}$ )  
276 and M-TiO<sub>2</sub> ( $118 \text{ m}^2 \text{ g}^{-1}$ ), and both are higher than that of M-P25 ( $65 \text{ m}^2 \text{ g}^{-1}$ ). The total pore  
277 volume ( $V_p$ ) was significantly higher for M-GOT when compared to M-TiO<sub>2</sub>, evidencing that  
278 a pronounced porosity is created when GO sheets and TiO<sub>2</sub> are in contact. The contact angles,  
279 also shown in Table 1, were very low for all membranes ( $<18^\circ$ ), indicating the high  
280 hydrophilicity of the membranes' surface. In particular, M-GOT presents the lowest contact  
281 angle ( $11^\circ$ ), which can be of relevance to treat high water fluxes.

282

### 283 *3.2. Removal of pollutants in dark phase*

284 Figure 3 shows DP and MO removals under dark conditions in filtration experiments  
285 performed using both DW and SBW at natural pH and 25 °C. The results are given for a  
286 period where saturation of all membranes was observed (60 min), and before starting to  
287 increase the concentration of pollutants in the reactor outlet.

288 These results indicate that there is a low removal of the pollutants (ca. 0.2%) when using the  
289 commercial MCE membrane in the dark regardless the liquid media (i.e. DW or SBW,  
290 respectively labelled as Blank\_DW or Blank\_SBW in Figure 3). Regarding the experiments  
291 with DW, DP removal was significantly higher for M-GOT (12%), M-TiO<sub>2</sub> (9%) and M-P25  
292 (3%) than for MCE. The same tendency was observed for MO, i.e. the highest MO removal  
293 was obtained with the M-GOT membrane (8%), lower DP removals being obtained with the  
294 other membranes, namely 6% with M-TiO<sub>2</sub> and 5% with M-P25. The removal of these  
295 pollutants can be related with two different phenomena occurring under dark conditions,  
296 adsorption or retention (Xu et al. 2013a). In order to discriminate between both, some

297 screening filtration experiments were performed (not shown) suggesting that the pollutant  
298 removal on the photocatalytic membranes may be attributed to DP adsorption.

299 Taking into account the speciation diagrams of both DP and MO (Figures 4a and 4b,  
300 respectively), the  $pK_a$  of DP and MO are ca. 8.9 (Hein and Jeannot 2001) and 4.2 (de Araujo  
301 et al. 2000), respectively. Since the pH in experiments with DW was near to 6.0 (5.9 for DP  
302 and 6.1 for MO), this means that DP is positively charged while MO is negatively charged  
303 under our experimental conditions. In addition, the  $pH_{PZC}$  of both bare  $TiO_2$  and GOT  
304 materials are ca. 3.1 and 2.9, respectively (Table 1). Therefore, M- $TiO_2$  and M-GOT  
305 membranes are expected to present negatively charged surfaces at the pH of the experiments  
306 (~ 6.0), explaining why the adsorption of DP is higher (electrostatic interactions) than in that  
307 of MO (electrostatic repulsions) when both membranes were employed. In the case of M-P25,  
308 MO removal was higher than DP removal in DW because the M-P25 membrane surface is  
309 practically uncharged ( $pH_{PZC}$  ca. 6.3) at the operating pH conditions (~ 6.0). Overall, the  
310 lower adsorption capacity for the M-P25 membrane compared to both M- $TiO_2$  and M-GOT  
311 membranes can be ascribed to  $S_{BET}$  (Table 1) which is higher for bare- $TiO_2$  and GOT (118  
312 and  $117 \text{ m}^2 \text{ g}^{-1}$ , respectively) than for P25 ( $65 \text{ m}^2 \text{ g}^{-1}$ ).

313 The effect of the presence of NaCl (SBW) on the removal of DP and MO under dark  
314 conditions is also shown in Figure 3. The results indicate that the presence of NaCl in water is  
315 not really affecting the adsorption of these pollutants onto the membranes, probably due to the  
316 low amount of  $Cl^-$  ions in the SBW prepared solutions ( $NaCl \text{ } 0.5 \text{ g L}^{-1}$ ). In addition, only ca.  
317 4-5% of the initial  $Cl^-$  concentration was removed during the filtration experiments under  
318 dark conditions (data not shown). The  $Cl^-$  ions are not retained in the membranes due to their  
319 (i) low molecular size (167 pm for the  $Cl^-$  ionic radius), (ii) competitive adsorption with the  
320 pollutant molecules, together with (iii) electrostatic repulsions in the case of M-GOT and M-  
321  $TiO_2$ .

322

### 323 3.3. DP photocatalytic degradation

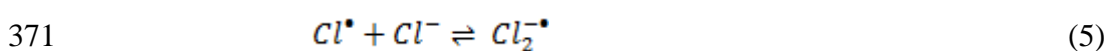
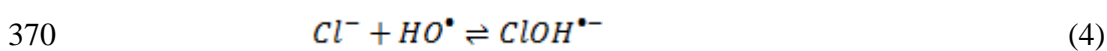
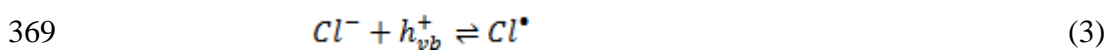
324 The efficiency of the membranes for the photocatalytic degradation of DP under near-UV/Vis  
325 (closed symbols) and visible light irradiation (open symbols) is shown in Figures 5a and 5b,  
326 respectively for DW and SBW, where  $C_0$  represents the DP concentration in the dark after  
327 180 min. It can be observed that the MCE membrane (Blank, cross symbol) did not have any  
328 photocatalytic performance by itself under near-UV/Vis (and also under visible light  
329 irradiation, not shown), using either DW or SBW, and that DP is a very refractory pollutant  
330 when irradiated in the absence of a catalyst, as previously reported (Pastrana-Martínez et al.  
331 2012). For comparison purposes, the experiments were carried out with the same irradiation  
332 lamp and pollutants tested by our group in slurry/batch mode (Pastrana-Martínez et al. 2013a,  
333 Pastrana-Martínez et al. 2014, Pastrana-Martínez et al. 2012). Although suspended  
334 photocatalysts can achieve the highest possible catalytic efficiency, the issue of separating the  
335 photocatalysts particles from the treated water was solved with the photocatalytic membranes.  
336 M-GOT and M-P25 are very active photocatalytic membranes, presenting comparable  
337 efficiencies under near-UV-Vis irradiation in terms of DP removal during the first  
338 photocatalytic cycle (ca. 73% in DW and ca. 60% in SBW). The lowest DP removal was  
339 obtained for M-TiO<sub>2</sub> (43% in DW and 39% in SBW). The same tendency was observed in  
340 terms of TOC removal in 240 min, i.e. M-P25, M-TiO<sub>2</sub> and M-GOT produced TOC  
341 reductions of 35%, 18% and 35%, respectively, in DW (Figure 5c).

342 The photocatalytic DP degradation under visible light illumination in DW (Figure 5a) was  
343 significantly higher for M-GOT (ca. 28%) than for TiO<sub>2</sub> membranes (ca. 5% with both M-  
344 TiO<sub>2</sub> and M-P25) indicating that TiO<sub>2</sub> is not active under visible light illumination, in  
345 agreement with previous reports where similar materials were used in the form of powder  
346 slurries for the photodegradation of different pollutants (Fotiou et al. 2013, Maroga Mboula et

347 al. 2013, Pastrana-Martínez et al. 2012). This observation confirms that the addition of GO  
 348 into the TiO<sub>2</sub> matrix increases light absorption in the visible spectral range, resulting from a  
 349 decrease in the band-gap energy (2.9, 3.1, and 3.2 eV for M-GOT, M-TiO<sub>2</sub> and M-P25,  
 350 respectively, Table 1). In our previous studies (Pastrana-Martínez et al. 2012, Pastrana-  
 351 Martínez et al. 2013b), the high activity of the GOT composite was attributed to the good  
 352 TiO<sub>2</sub> distribution in the composite containing ca. 4% of GO content, leading to good assembly  
 353 and interfacial coupling between the GO sheets and TiO<sub>2</sub> nanoparticles (as can be observed in  
 354 the SEM micrograph of M-GOT, Figure 2f).

355 Regarding the results with SBW (Figure 5b), it can be concluded that the presence of NaCl  
 356 (0.5 g L<sup>-1</sup>) slightly decreases the photocatalytic efficiency for DP under near-UV/Vis (i.e.  
 357 60%, 39% and 61% for M-P25, M-TiO<sub>2</sub> and M-GOT, respectively in the first cycle), in  
 358 comparison with DW (Figure 5a). TOC removal (Figure 5c) follows a trend similar to that  
 359 observed for DP degradation, i.e. lower mineralizations were also obtained in the presence of  
 360 NaCl (27%, 12% and 28% for M-P25, M-TiO<sub>2</sub> and M-GOT, respectively).

361 This effect could be due to the presence of Cl<sup>-</sup> ions acting as holes and hydroxyl radical  
 362 scavengers, affecting the efficiency of the photocatalytic process. The presence of Cl<sup>-</sup> anions  
 363 in SBW could generate less reactive species such as chlorine radicals (Cl•) and dichloride  
 364 anion radicals (Cl<sub>2</sub><sup>-•</sup>) (Eqs. 3-5), which are less reactive than HO• radicals (De Laat and Le  
 365 2006). The formation of these less reactive species may decrease the efficiency of the process.  
 366 These results are in agreement with those published in literature (Sirtori et al. 2010, Yap and  
 367 Lim 2011), where a negative effect of Cl<sup>-</sup> ions was observed for the photocatalytic  
 368 degradation of other pollutants.



372 ...Membrane cleaning will be an essential part during the photocatalytic degradation of  
373 organic pollutants in salty water. Different cleaning methods have been proposed in  
374 literature (Shi et al. 2014, Wang et al. 2014) such as physical, chemical and  
375 biological/biochemical cleaning according to fouling removal mechanisms or cleaning agents  
376 used

377

### 378 *3.4. MO photocatalytic degradation*

379 The same type of photocatalytic experiments were performed using MO as model pollutant.  
380 The photocatalytic activity of M-P25, M-TiO<sub>2</sub> and M-GOT membranes under both near-  
381 UV/Vis and visible light irradiation are shown in Figures 6a and 6b for DW and SBW,  
382 respectively. It is observed that MO is poorly removed when the commercial MCE membrane  
383 is used (Blank). The M-GOT membrane showed significantly higher photocatalytic activity  
384 for MO abatement than the other membranes tested in DW (51% and 5% for M-P25, 39% and  
385 4% for M-TiO<sub>2</sub>, 65% and 19% for M-GOT, under near-UV/Vis and visible light irradiation,  
386 respectively). The same trend was found concerning the respective TOC removal (Figure 6c).  
387 The photodegradation of MO from the first to the second cycle was practically the same for  
388 all membranes when using DW as solvent (Figure 6a).

389 For the experiments with SBW (Figure 6b), once again the membrane prepared with the GOT  
390 composite exhibited the highest photocatalytic activity under near-UV/Vis and visible light  
391 irradiation (respectively, 52% and 13% reduction of the initial MO concentration) and also the  
392 highest TOC removal (respectively, 31% and 9%, Figure 6c). However, the presence of NaCl  
393 leads to a slight decrease in MO degradation, in comparison with DW, regardless of the  
394 membranes employed (Figure 6b). The same trend was observed in terms of TOC removal  
395 (Figure 6c). As previously observed for DP removal, MO degradation decreases from the first  
396 to the second bright cycle, reinforcing the idea that Cl<sup>-</sup> ions are scavengers of holes and



397 hydroxyl radicals.

398

### 399 *3.5. Permeate flux and anti-fouling of the photocatalytic membranes*

400 Regardless of the membrane employed, the photocatalytic degradation of both pollutants  
401 tested was practically the same from the first to the second bright cycle when using DW as  
402 solvent (Figures 5a and 6a for DP and MO, respectively). These results indicate that all  
403 membranes are quite stable and that fouling did not take place. This observation also suggests  
404 that parent pollutants/intermediate compounds are not irreversibly accumulated on the  
405 membrane surface, which guarantees that the membranes can maintain high permeate fluxes  
406 for long operation periods (Zhang et al. 2014a).

407 The permeate flux was monitored for experiments performed with DP. Figures 7a and 7b  
408 show the results obtained for DW and SBW, respectively, in 240 min. The flux performance  
409 of the MCE membrane (blank) in darkness, UV/Vis and visible light irradiation, did not  
410 change during the experiments. In addition, the permeate flux of the lab-made membranes  
411 (M-P25, M-TiO<sub>2</sub> and M-GOT) was slightly lower in comparison with that of the blank MCE  
412 membrane, probably due to the nanostructured materials that were deposited over MCE and  
413 that have influence on the membranes porosity.

414 The pollutants can stay adsorbed on the membrane surface and can partially block the pores  
415 under dark conditions. The permeate flux increased for M-P25, M-TiO<sub>2</sub> and M-GOT  
416 membranes under near-UV/Vis irradiation, probably as a consequence of the photocatalytic  
417 degradation of DP molecules adsorbed on the membrane surface or to a higher hydrophilicity  
418 of the materials under near-UV/Vis irradiation. However, a similar increase of the water flux  
419 was not always observed under visible light illumination. Only for M-GOT the permeate flux  
420 was higher at such conditions than in the darkness, which can be related to the high  
421 photocatalytic activity of this membrane under visible illumination, when compared with the

422 others (Figure 7), and/or to its higher hydrophilicity (contact angles of 11°, 17° and 18° for M-  
423 GOT, M-TiO<sub>2</sub> and M-P25, respectively). Therefore, overall, M-GOT performs better than M-  
424 TiO<sub>2</sub> and M-P25.

425

### 426 *3.6. Hierarchically ordered M-GO/GOT membrane*

427 A free-standing GO membrane (M-GO) was introduced between the commercial MCE  
428 membrane and the GOT layer with the aim to improve the performance of the M-GOT  
429 membrane. The resulting membrane was referred as M-GO/GOT and its efficiency was  
430 evaluated for the degradation of DP, first in darkness and then under visible and near-UV/Vis  
431 irradiation. The experiments were carried out using DW and simulated seawater (SSW - 35 g  
432 L<sup>-1</sup> NaCl).

433 The cross-sectional SEM micrographs of the prepared M-GO/GOT membrane are shown in  
434 Figure 8. Uniform GO layers (ca. 6.5 μm of total thickness) between the MCE membrane and  
435 the GOT photocatalyst are observed. The GO membrane consists of several GO sheets (inset  
436 of Figure 8b: M-GO) and the GOT catalyst was homogeneously deposited on top of M-GO.  
437 The M-GO/GOT membrane has an overall thickness of ~ 200 μm, in which ~ 50 - 55 μm are  
438 due to the GOT photocatalyst. The thickness of the GOT layer in M-GO/GOT seems to be  
439 smaller than in the case of M-GOT (65 μm), both prepared with the same amount of  
440 photocatalyst. This smaller thickness could be due to a stronger packing of the GOT particles  
441 during the preparation step, since a longer time of filtration was required to prepare M-  
442 GO/GOT.

443 Figures 9a and 9b show the results obtained in terms of DP removal and permeate flux,  
444 respectively. The M-GO/GOT membrane exhibited a significantly higher DP removal under  
445 dark conditions in DW when compared to M-GOT (i.e, 12 and 42% for M-GOT and M-  
446 GO/GOT, respectively). The DP concentration increased after the initial fast DP removal and

447 before turning on the lamp, but a long dark period (up to 48 hours) was needed for the  
448 saturation of the M-GO-GOT membrane with the DP pollutant while only 180 min were  
449 required in the case of the M-GOT membrane.

450 These results indicate that the adsorption and/or exclusion of pollutants of the M-GOT  
451 membrane was increased by the introduction of the free-standing GO membrane, the M-  
452 GO/GOT membrane presenting a higher DP adsorption capacity in the filtration process. As  
453 expected, the removal capacity was lower when the experiments were performed in SSW  
454 (10%) due to the high content of  $\text{Cl}^-$  anions ( $35 \text{ g L}^{-1}$ ) that could reduce the electrostatic  
455 interactions between catalysts and pollutants due to a screening effect (Stuart et al. 1991), i.e.  
456 the  $\text{Cl}^-$  anions might pair with the positive DP molecules and reduce the electrostatic  
457 interactions with the catalyst surface, and/or could block the active sites of the catalyst  
458 (Kamble et al. 2008).

459 Regarding photocatalytic activity, the M-GO/GOT membrane also showed a relatively good  
460 activity for DP degradation under near-UV/Vis and visible light irradiation; however, the M-  
461 GOT membrane performed better (Figures 5a and 5b respectively). Since the thickness of the  
462 GOT layer in M-GO/GOT was smaller ( $\sim 50 - 55 \mu\text{m}$ ) than in the case of M-GOT ( $65 \mu\text{m}$ ),  
463 one possible explanation is that the photocatalyst is more compacted in the case of M-  
464 GO/GOT and, therefore, less exposed to the irradiation, an important aspect when dealing  
465 with photocatalytic reactors. The longer time of filtration required by the presence of GO is  
466 the main synthesis limitation regarding this issue. The permeate flux increased for the M-  
467 GOT membrane under near-UV/Vis and visible light irradiation (Figure 7), probably as a  
468 consequence of the photocatalytic degradation of DP molecules adsorbed on the membrane  
469 surface, or to a higher hydrophilicity of the materials under irradiation. The permeate flux was  
470 also monitored for the M-GO/GOT membrane in darkness and under visible and near-UV/Vis  
471 irradiation (Figure 9b). As expected, the results showed a decrease of the permeate flux under

472 dark conditions. However, an increase in permeate flux was subsequently observed under  
473 visible light and near-UV/Vis irradiation, as in the case of M-GOT. This effect was more  
474 significant for the experiments in DW, and can be attributed to the photocatalytic activity,  
475 hydrophilicity and anti-fouling properties of the prepared membranes.

476

#### 477 **4. Conclusions**

478 Different photocatalytic membranes were synthesized with P25 (M-P25), bare-TiO<sub>2</sub> (M-TiO<sub>2</sub>)  
479 and GO-TiO<sub>2</sub> composite. The prepared membranes were compared in terms of photocatalytic  
480 activity using distilled water and simulated brackish water and seawater. The photocatalysts  
481 were homogeneously deposited without appreciable presence of cracks, holes or another  
482 defects. All the membranes presented high activity and stability in consecutive light-dark  
483 cycles under continuous mode. During the photocatalytic reaction, the permeate flux  
484 increased due to the high hydrophilicity of the membranes and larger contaminant removal by  
485 photodegradation. The presence of NaCl had a substantially detrimental effect on the  
486 photocatalytic performance which may be due to the chloride anions acting as hole and  
487 hydroxyl radical scavengers. In general, the M-GOT membrane showed significantly higher  
488 photocatalytic activity for the pollutants abatement than the other membranes tested. In  
489 addition, an innovative hierarchically membrane referred as M-GO/GOT was prepared by  
490 intercalating a GO membrane in the structure of the M-GOT. This membrane showed higher  
491 pollutant removal under dark conditions and good performance under visible and near-  
492 UV/Vis irradiations. However, the M-GOT membrane performed better, probably due to the  
493 higher compactness in the case of M-GO/GOT as a consequence of the synthesis conditions  
494 required for its preparation.

495

#### 496 **Acknowledgements**

497 Financial support for this work was provided by projects PTDC/AAC-AMB/122312/2010 co-  
498 financed by FCT (Fundação para a Ciência e a Tecnologia) and FEDER (Fundo Europeu de  
499 Desenvolvimento Regional) through Programme COMPETE (FCOMP-01-0124-FEDER-  
500 019503). This work was also partially co-financed by FCT and FEDER through project PEst-  
501 C/EQB/LA0020/2013 (COMPETE), and by QREN, ON2 (Programa Operacional do Norte)  
502 and FEDER through projects NORTE-07-0124-FEDER-000015 and NORTE-07-0202-  
503 FEDER-038900. LMPM and SMT acknowledge financial support from FCT grants  
504 SFRH/BPD/88964/2012 and SFRH/BPD/74239/2010, respectively. AMTS acknowledges the  
505 FCT Investigator 2013 Programme (IF/01501/2013), with financing from the European Social  
506 Fund and the Human Potential Operational Programme. Technical assistance by Dr. Carlos Sá  
507 and CEMUP team with SEM analysis is gratefully acknowledged.

508

## 509 **References**

510 Albu, S.P., Ghicov, A., Macak, J.M., Hahn, R. and Schmuki, P. (2007) Self-Organized, Free-  
511 Standing TiO<sub>2</sub> Nanotube Membrane for Flow-through Photocatalytic Applications. *Nano Lett.*  
512 7(5), 1286-1289.

513 Amalraj Appavoo, I., Hu, J., Huang, Y., Li, S.F.Y. and Ong, S.L. (2014) Response surface  
514 modeling of Carbamazepine (CBZ) removal by Graphene-P25 nanocomposites/UVA process  
515 using central composite design. *Water Res.* 57(0), 270-279.

516 Athanasekou, C.P., Morales-Torres, S., Likodimos, V., Romanos, G.E., Pastrana-Martinez,  
517 L.M., Falaras, P., Dionysiou, D.D., Faria, J.L., Figueiredo, J.L. and Silva, A.M.T. (2014)  
518 Prototype composite membranes of partially reduced graphene oxide/TiO<sub>2</sub> for photocatalytic  
519 ultrafiltration water treatment under visible light. *Appl. Catal. B* 158–159(0), 361-372.

520 Baek, Y., Kim, C., Seo, D.K., Kim, T., Lee, J.S., Kim, Y.H., Ahn, K.H., Bae, S.S., Lee, S.C.,  
521 Lim, J., Lee, K. and Yoon, J. (2014) High performance and antifouling vertically aligned  
522 carbon nanotube membrane for water purification. *J. Membr. Sci.* 460(0), 171-177.

523 Barrett, E.P., Joyner, L.G. and Halenda, P.P. (1951) The Determination of Pore Volume and  
524 Area Distributions in Porous Substances. I. Computations from Nitrogen Isotherms. *J. Am.*  
525 *Chem. Soc.* 73(1), 373-380.

526 Brunauer, S., Emmett, P.H. and Teller, E. (1938) Adsorption of Gases in Multimolecular  
527 Layers. *J. Am. Chem. Soc.* 60(2), 309-319.

528 Cui, Z., Hassankiadeh, N.T., Lee, S.Y., Lee, J.M., Woo, K.T., Sanguineti, A., Arcella, V.,  
529 Lee, Y.M. and Drioli, E. (2013) Poly(vinylidene fluoride) membrane preparation with an  
530 environmental diluent via thermally induced phase separation. *J. Membr. Sci.* 444(0), 223-  
531 236.

532 Chen, X. and Mao, S.S. (2007) Titanium Dioxide Nanomaterials: Synthesis, Properties,  
533 Modifications, and Applications. *Chem. Rev.* 107(7), 2891-2959.

534 Das, R., Ali, M.E., Hamid, S.B.A., Ramakrishna, S. and Chowdhury, Z.Z. (2014) Carbon  
535 nanotube membranes for water purification: A bright future in water desalination.  
536 *Desalination* 336(0), 97-109.

537 de Araujo, R.E., Gomes, A.S.L. and de Araújo, C.B. (2000) Measurements of pKa of organic  
538 molecules using third-order nonlinear optics. *Chem. Phys. Lett.* 330(3-4), 347-353.

539 De Laat, J. and Le, T.G. (2006) Effects of chloride ions on the iron(III)-catalyzed  
540 decomposition of hydrogen peroxide and on the efficiency of the Fenton-like oxidation  
541 process. *Appl. Catal. B* 66(1-2), 137-146.

542 Dreyer, D.R., Park, S., Bielawski, C.W. and Ruoff, R.S. (2010) The chemistry of graphene  
543 oxide. *Chem. Soc. Rev.* 39(1), 228-240.

544 Fan, W., Lai, Q., Zhang, Q. and Wang, Y. (2011) Nanocomposites of TiO<sub>2</sub> and Reduced  
545 Graphene Oxide as Efficient Photocatalysts for Hydrogen Evolution. *J. Phys. Chem. C*  
546 115(21), 10694-10701.

547 Fotiou, T., Triantis, T.M., Kaloudis, T., Pastrana-Martínez, L.M., Likodimos, V., Falaras, P.,  
548 Silva, A.M.T. and Hiskia, A. (2013) Photocatalytic Degradation of Microcystin-LR and Off-  
549 Odor Compounds in Water under UV-A and Solar Light with a Nanostructured Photocatalyst  
550 Based on Reduced Graphene Oxide–TiO<sub>2</sub> Composite. Identification of Intermediate Products.  
551 *Ind. Eng. Chem. Res.* 52(39), 13991-14000.

552 Gao, P., Liu, Z., Tai, M., Sun, D.D. and Ng, W. (2013) Multifunctional graphene oxide–TiO<sub>2</sub>  
553 microsphere hierarchical membrane for clean water production. *Appl. Catal. B* 138–139(0),  
554 17-25.

555 Gao, Y., Hu, M. and Mi, B. (2014) Membrane surface modification with TiO<sub>2</sub>–graphene  
556 oxide for enhanced photocatalytic performance. *J. Membr. Sci.* 455(0), 349-356.

557 Hein, J. and Jeannot, M. (2001) Drug Distribution: A Guided-Inquiry Laboratory Experiment  
558 in Coupled Homogeneous and Heterogeneous Equilibria. *J. Chem. Educ.* 78(2), 224.

559 Huang, X., Wang, L., Zhou, J. and Gao, N. (2014) Photocatalytic decomposition of bromate  
560 ion by the UV/P25-Graphene processes. *Water Res.* 57(0), 1-7.

561 Hummers, W.S. and Offeman, R.E. (1958) Preparation of Graphitic Oxide. *J. Am. Chem.*  
562 *Soc.* 80(6), 1339-1339.

563 Kamble, S.P., Mangrulkar, P.A., Bansiwala, A.K. and Rayalu, S.S. (2008) Adsorption of  
564 phenol and o-chlorophenol on surface altered fly ash based molecular sieves. *Chem. Eng. J.*  
565 138(1–3), 73-83.

566 Kim, J. and Van der Bruggen, B. (2010) The use of nanoparticles in polymeric and ceramic  
567 membrane structures: Review of manufacturing procedures and performance improvement for  
568 water treatment. *Environ. Pollut.* 158(7), 2335-2349.

569 Long, M., Qin, Y., Chen, C., Guo, X., Tan, B. and Cai, W. (2013) Origin of Visible Light  
570 Photoactivity of Reduced Graphene Oxide/TiO<sub>2</sub> by in Situ Hydrothermal Growth of  
571 Undergrown TiO<sub>2</sub> with Graphene Oxide. *J. Phys. Chem. C* 117(32), 16734-16741.

572 Maim, C.J., Genung, L.B. and Fleckenstein, J.V. (1947) Densities of Cellulose Esters. *Ind.*  
573 *Eng. Chem. Res.* 39(11), 1499-1504.

574 Maroga Mboula, V., Héquet, V., Andrès, Y., Pastrana-Martínez, L.M., Doña-Rodríguez, J.M.,  
575 Silva, A.M.T. and Falaras, P. (2013) Photocatalytic degradation of endocrine disruptor  
576 compounds under simulated solar light. *Water Res.* 47(12), 3997-4005.

577 Morales-Torres, S., Silva, T.L.S., Pastrana-Martinez, L.M., Brandao, A.T.S.C., Figueiredo,  
578 J.L. and Silva, A.M.T. (2014) Modification of the surface chemistry of single- and multi-  
579 walled carbon nanotubes by HNO<sub>3</sub> and H<sub>2</sub>SO<sub>4</sub> hydrothermal oxidation for application in  
580 direct contact membrane distillation. *Phys. Chem. Chem. Phys.* 16(24), 12237-12250.

581 Pan, J.H., Zhang, X., Du, A.J., Sun, D.D. and Leckie, J.O. (2008) Self-Etching Reconstruction  
582 of Hierarchically Mesoporous F-TiO<sub>2</sub> Hollow Microspherical Photocatalyst for Concurrent  
583 Membrane Water Purifications. *J. Am. Chem. Soc.* 130(34), 11256-11257.

584 Pastrana-Martínez, L.M., Morales-Torres, S., Kontos, A.G., Moustakas, N.G., Faria, J.L.,  
585 Doña-Rodríguez, J.M., Falaras, P. and Silva, A.M.T. (2013a) TiO<sub>2</sub>, surface modified TiO<sub>2</sub>  
586 and graphene oxide-TiO<sub>2</sub> photocatalysts for degradation of water pollutants under near-  
587 UV/Vis and visible light. *Chem. Eng. J.* 224(0), 17-23.

588 Pastrana-Martínez, L.M., Morales-Torres, S., Likodimos, V., Falaras, P., Figueiredo, J.L.,  
589 Faria, J.L. and Silva, A.M.T. (2014) Role of oxygen functionalities on the synthesis of  
590 photocatalytically active graphene-TiO<sub>2</sub> composites. *Appl. Catal. B* 158-159(0), 329-340.

591 Pastrana-Martínez, L.M., Morales-Torres, S., Likodimos, V., Figueiredo, J.L., Faria, J.L.,  
592 Falaras, P. and Silva, A.M.T. (2012) Advanced nanostructured photocatalysts based on



593 reduced graphene oxide–TiO<sub>2</sub> composites for degradation of diphenhydramine pharmaceutical  
594 and methyl orange dye. *Appl. Catal. B* 123–124(0), 241-256.

595 Pastrana-Martínez, L.M., Morales-Torres, S., Papageorgiou, S.K., Katsaros, F.K., Romanos,  
596 G.E., Figueiredo, J.L., Faria, J.L., Falaras, P. and Silva, A.M.T. (2013b) Photocatalytic  
597 behaviour of nanocarbon–TiO<sub>2</sub> composites and immobilization into hollow fibres. *Appl.*  
598 *Catal. B* 142–143(0), 101-111.

599 Pendergast, M.M. and Hoek, E.M.V. (2011) A review of water treatment membrane  
600 nanotechnologies. *Energy Environ. Sci.* 4(6), 1946-1971.

601 Peters, T. (2010) Membrane Technology for Water Treatment. *Chem. Eng. Technol.* 33(8),  
602 1233-1240.

603 Rouquerol, F., Rouquerol, J. and Sing, K.S.W. (1999) Adsorption by Powders and Porous  
604 Solids. Principles, Methodology and Applications, Academic Press, London.

605 Shannon, M.A., Bohn, P.W., Elimelech, M., Georgiadis, J.G., Marinas, B.J. and Mayes, A.M.  
606 (2008) Science and technology for water purification in the coming decades. *Nature*  
607 452(7185), 301-310.

608 Shi, X., Tal, G., Hankins, N.P. and Gitis, V. (2014) Fouling and cleaning of ultrafiltration  
609 membranes: A review. *Journal of Water Process Engineering* 1, 121-138.

610 Sirtori, C., Agüera, A., Gernjak, W. and Malato, S. (2010) Effect of water-matrix composition  
611 on Trimethoprim solar photodegradation kinetics and pathways. *Water Res.* 44(9), 2735-  
612 2744.

613 Stuart, M.A.C., Fler, G.J., Lyklema, J., Norde, W. and Scheutjens, J.M.H.M. (1991)  
614 Adsorption of Ions, Polyelectrolytes and Proteins. *Adv. Colloid Interface Sci.* 34(0), 477-535.

615 Tu, W., Zhou, Y. and Zou, Z. (2013) Versatile Graphene-Promoting Photocatalytic  
616 Performance of Semiconductors: Basic Principles, Synthesis, Solar Energy Conversion, and  
617 Environmental Applications. *Adv. Funct. Mater.* 23(40), 4996-5008.

618 Ulbricht, M. (2006) Advanced functional polymer membranes. *Polymer* 47(7), 2217-2262.

619 Wang, Z., Ma, J., Tang, C.Y., Kimura, K., Wang, Q. and Han, X. (2014) Membrane cleaning  
620 in membrane bioreactors: A review. *J. Membr. Sci.* 468, 276-307.

621 Xu, C., Cui, A., Xu, Y. and Fu, X. (2013a) Graphene oxide–TiO<sub>2</sub> composite filtration  
622 membranes and their potential application for water purification. *Carbon* 62(0), 465-471.

623 Xu, J., Chang, C.Y., Hou, J. and Gao, C. (2013b) Comparison of approaches to minimize  
624 fouling of a UF ceramic membrane in filtration of seawater. *Chem. Eng. J.* 223(0), 722-728.

625 Yap, P.S. and Lim, T.T. (2011) Effect of aqueous matrix species on synergistic removal of  
626 bisphenol-A under solar irradiation using nitrogen-doped TiO<sub>2</sub>/AC composite. *Appl. Catal. B*  
627 101(3–4), 709-717.

628 Zhang, H., Quan, X., Chen, S. and Zhao, H. (2006) Fabrication and Characterization of  
629 Silica/Titania Nanotubes Composite Membrane with Photocatalytic Capability. *Environ. Sci.*  
630 *Technol.* 40(19), 6104-6109.

631 Zhang, X., Wang, D.K. and Diniz da Costa, J.C. (2014a) Recent progresses on fabrication of  
632 photocatalytic membranes for water treatment. *Catal. Today* 230(0), 47-54.

633 Zhang, X., Wang, D.K., Lopez, D.R.S. and Diniz da Costa, J.C. (2014b) Fabrication of  
634 nanostructured TiO<sub>2</sub> hollow fiber photocatalytic membrane and application for wastewater  
635 treatment. *Chem. Eng. J.* 236(0), 314-322.

636